

## Simulation of failure in porous elastic solids incorporating size effects

Uwe Mühlich<sup>1a</sup>, Lutz Zybell<sup>2b</sup> and Meinhard Kuna<sup>3c</sup>

<sup>123</sup>TU-Bergakademie Freiberg, IMFD, Lampadiusstrasse 4, Freiberg 09599, Germany

<sup>a</sup>[Uwe.Muehlich@imfd.tu-freiberg.de](mailto:Uwe.Muehlich@imfd.tu-freiberg.de), <sup>b</sup>[Lutz.Zybell@imfd.tu-freiberg.de](mailto:Lutz.Zybell@imfd.tu-freiberg.de),

<sup>c</sup>[Meinhard.Kuna@imfd.tu-freiberg.de](mailto:Meinhard.Kuna@imfd.tu-freiberg.de)

**Keywords:** strain gradient elasticity, homogenization, size effect, failure

**Abstract.** A first order strain gradient elasticity model in conjunction with a simple failure criterion is employed in order to discuss size effects in failure of porous elastic materials. The model contains two micro structural parameters: namely the void volume fraction  $f$  and the mean of the half void spacing  $R$ . Three different examples: a plate with a hole under remote uniaxial and biaxial tension and a compression test using a long cylindrical bar are considered. The numerical simulations were performed varying  $f$  and  $R$  in order to investigate the influence of different microstructural dimensions on the onset of macroscopic failure. A size effect can be observed where the results indicate that this size effect does not only depend on the ratio between macroscopic and microstructural dimensions but also on the macroscopic geometry and loading conditions.

### Introduction

Size effects in failure of porous elastic solids are evidenced by a large number of experimental studies. These investigations always indicate a certain relationship between the failure load and the ratio between the macroscopic and microstructural dimensions like e.g. grain size, defect spacing, etc. of the considered body, where the microstructural dimensions are determined by the material. A detailed discussion would go beyond the scope of this paper. Therefore, we refer without appraisal only to [1-3].

In order to apply a continuous description at the macrolevel which accounts to a certain extent for the influence of the materials microstructure, homogenization methods based on the concept of the representative volume element (RVE) have been developed within the scope of classical continuum mechanics, i.e. within the framework of the theory of simple materials. However, since only specific values enter the resulting models, size effects cannot be reproduced. With respect to the class of materials considered here, this means that these continuum models cannot distinguish between a material with many small micro-voids and another material with less but bigger micro-voids as long as the specific void volume fraction is the same.

On the other hand, a first order strain gradient elasticity theory was developed by Mindlin [4,5] based on an earlier contribution of Toupin [6]. Due to the presence of the strain gradients, additional length parameters appear and therefore size effects can be reproduced. Furthermore, continuum models fitting into Mindlin's framework can be transparently obtained by higher order homogenization, i.e. homogenization with more complex conditions prescribed at the outer boundary of the RVE.

In this paper, materials whose micro structure is characterized by long cylindrical voids surrounded by linear elastic matrix material are considered. First order strain gradient theory is applied where the constitutive equations have been derived by Zybell et al. in [7] by employing the higher order homogenization procedure proposed by Gologanu [8] and further investigated by Forest [9]. The only microstructural parameters of the model are the void volume fraction  $f$  and the mean of the half void spacing  $R$ . A simple failure criterion based on the hoop stress at the boundary of the micro-voids has been derived. The strain gradient model has been implemented into the commercial finite-

element program ABAQUS [10] using a mixed formulation as proposed by Shu et al. [11]. The implementation is described in detail in Zybelle [12].

Numerical simulations were performed considering two different macroscopic geometries and varying  $f$  and  $R$  in order to investigate the influence of different microstructural dimensions on the onset of macroscopic failure.

The paper is organized as follows. The following section considers briefly the essentials of the strain gradient theory developed in [4,5]. The homogenization procedure and the failure criteria are outlined. In the second part, the geometry and loading conditions of the considered examples are described and the results obtained by the numerical simulations are presented. Finally, some perspectives for further developments are given.

In the sequel, index notation together with the summation convention is used and capital letters represent macroscopic variables. Macroscopic and microscopic variables depend on the macroscopic coordinates  $X_i$  and the microscopic coordinates  $x_i$ , respectively. The abbreviation  $(\cdot)_{,i}$  indicates the partial derivative of the considered quantity  $(\cdot)$  with respect to the corresponding spatial coordinate.

### Strain gradient elasticity

Strain gradient elasticity may be formulated by the following set of equations for the macroscopic field variables

*Equilibrium conditions:*

$$(\Sigma_{ij,j} - M_{ijk,k})_{,j} = 0 \quad (1)$$

*Kinematic relations:*

$$E_{ij} = \frac{1}{2} (U_{i,j} + U_{j,i}) \quad (2)$$

$$H_{ijk} = \frac{1}{2} (U_{i,jk} + U_{j,ik}) \quad (3)$$

*Constitutive relations:*

$$\Sigma_{ij} = C_{ijkl} E_{kl} \quad (4)$$

$$M_{ijk} = D_{ijklmn} H_{lmn} \quad (5)$$

for all macroscopic points  $X$  of the considered body  $B$ , where  $U_i$  are the components of the displacement vector. The stresses  $\Sigma_{ij}$  and the higher order stresses  $M_{ijk}$  are related to their work conjugate kinematic variables, the strains  $E_{ij}$  and the strain gradients  $H_{ijk}$ , by the fourth and sixth order tensors  $\underline{C}$  and  $\underline{D}$ , respectively. The boundary value problem at the macro level is completely defined if in addition to Eq. 1 – Eq. 5 the following natural boundary conditions

$$T_i = T_i^* \quad X \in \partial B_T \quad (6)$$

$$R_i = 0_i \quad X \in \partial B_R \quad (7)$$

as well as the essential boundary conditions

$$U_i = U_i^* \quad X \in \partial B_U \tag{8}$$

$$N_p U_{i,p} = V_i^* \quad X \in \partial B_V \tag{9}$$

are taken into account, where variables marked with an asterisk (\*) indicate prescribed values. In general, higher order tractions different from zero could be prescribed at the boundary  $\partial B_R$ . However, in view of the applications for which the model will be used, this case is excluded here as indicated by Eq. 7. The surface tractions  $T_i$  and the higher order surface tractions  $R_i$  are given by

$$T_i = N_j (\Sigma_{ij} - M_{kji,k}) - D_j (N_k M_{kji}) + (D_l N_l) N_k N_j M_{kji} \tag{10}$$

$$R_i = N_k N_j M_{kji}, \tag{11}$$

where  $N_i$  and  $D_i$  are the components of the unit normal vector and the surface gradient, respectively. The model has been implemented into the finite element program ABAQUS using a mixed formulation. However, following [Shu et al.] an equivalent formulation based on the second gradients of the displacements was used for the implementation instead of the model given by Eq. 1 – Eq. 5.

### Constitutive equations for plane porous strain gradient elasticity

The components of the constitutive tensors  $\underline{C}$  and  $\underline{D}$  have been determined by higher order homogenization, where  $\underline{C}$  corresponds to the overall elasticity tensor of the theory of simple materials. The homogenization has been performed considering a cylindrical volume element (RVE) which consists of a cylindrical void surrounded by linear elastic matrix material as shown in Fig. 1. Plane stress and plane strain conditions have been assumed and quadratic boundary displacements related to the macroscopic strains and strain gradients have been prescribed at the outer boundary of the RVE.

$$u_i (r=R, \varphi) = E_{ik} x_k + \frac{1}{2} K_{ijk} x_j x_k - \frac{1}{2} (K_{ijk} + K_{jki}) X_k x_j \tag{12}$$

with

$$K_{ijk} = H_{ijk} - H_{ijk} + H_{kij}. \tag{13}$$

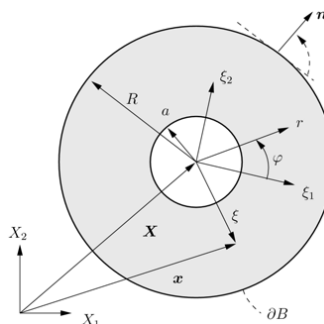


Figure 1: Representative Volume Element (RVE) for the homogenization procedure

At the inner boundary, the tractions must vanish

$$\Sigma_{ij}(r=a, \varphi)n_j = 0_i. \tag{14}$$

The boundary value problem for the RVE was solved analytically using Airy's-Stress function in conjunction with Fourier series in order to derive the microscopic stresses  $\sigma_{ij}$  and strains  $\varepsilon_{ij}$  inside the RVE as functions of the macroscopic strains and strain gradients, respectively, from which the components of  $\underline{C}$  and  $\underline{D}$  can be determined. More detailed information is given in [7].

The components of  $\underline{C}$  and  $\underline{D}$  depend on the void volume fraction  $f$  and the elasticity constants of the matrix material  $E$  and  $\nu$ . The components of  $\underline{D}$ , however, depend as well on the mean of the half void spacing  $R$ .

After solving the boundary value problem at the macro level, the macroscopic strains and strain gradients are known for every macroscopic point  $X$ . Furthermore, the microscopic stress and strain fields inside the corresponding RVE are known as well. In order to obtain a failure criterion, it is postulated that failure occurs if the hoop stress at the micro-void,  $\sigma_{\varphi\varphi}(r=a, \varphi)$ , reaches a critical value. This assumption includes actually two failure criteria. Failure by tension occurs if the maximum positive hoop stress  $\sigma_{\varphi\varphi}^{\max+}$  reaches a critical value and failure by compression takes place if the minimum negative hoop stress  $\sigma_{\varphi\varphi}^{\max-}$  becomes lower than or equal to a critical value. Both criteria are used in the following in order to predict the onset of failure of porous elastic solids.

### Numerical Examples

First, a cylindrical hole surrounded by a linear elastic strain gradient material under remote uniaxial tension in plane strain is considered.

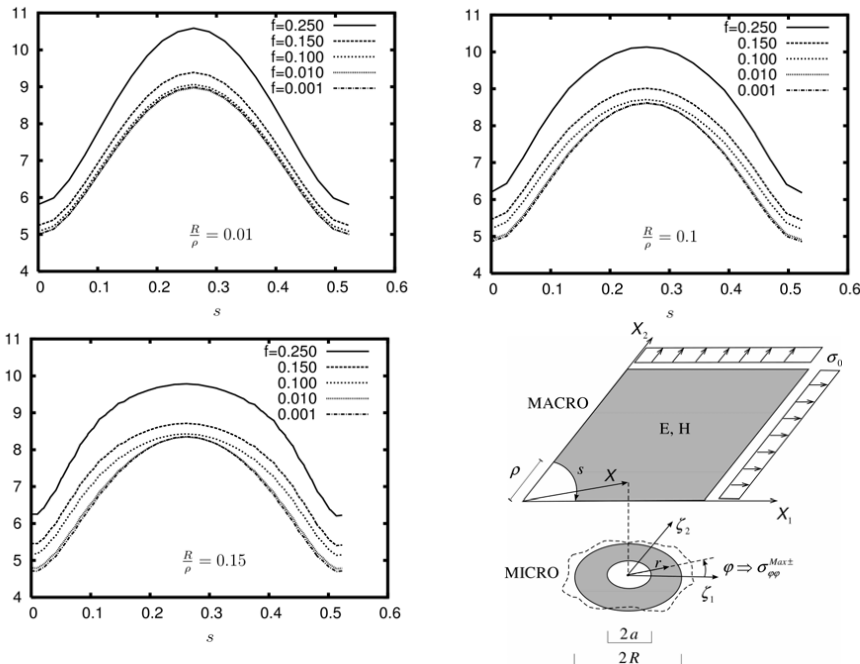


Figure 3:  $\sigma_{\varphi\varphi}^{\max+}/\sigma_0$  for biaxial remote tension as function of the arc length  $s$ , varying  $f$  and  $R/\rho$

Due to the symmetry of the problem, only a quarter of the geometry has to be modeled as shown in the lower right picture of Fig. 3.

With respect to the elasticity constants  $E$  and  $\nu$ , the values  $E=1000$  MPa and  $\nu=0.3$  were used for all calculations. However, different materials microstructures characterized by the void volume fraction  $f$  and the half void spacing  $R$  were considered. The values for the void volume fraction  $f$  were taken from the set (0.001, 0.010, 0.1, 0.150, 0.250) and the ratios between the half spacing of the microscopic voids  $R$  and the radius of the macroscopic hole  $\rho$  were chosen equal to  $R/\rho=0.01$ , 0.1 and 0.15.

For a given void volume fraction  $f$ , small and large values for  $R/\rho$  reflect micro structures with many small voids and micro structures with less but bigger voids, respectively.

The results for  $\sigma_{\varphi\varphi}^{\max+}$  along the boundary of the macroscopic hole are shown in Fig. 3 as functions of the arc length  $s$  for different micro structures. As it can be seen,  $\sigma_{\varphi\varphi}^{\max+}/\sigma_0$  decreases as  $R/\rho$  increases and in addition the curves become smoother with increasing  $R/\rho$ . Therefore, the failure criterion predicts that the onset of failure occurs at lower applied loads if the material has a dense micro structure ( $R/\rho$  small), compared with the case of a coarse micro structure ( $R/\rho$  large). Similar results were obtained for  $\sigma_{\varphi\varphi}^{\max-}$ .

Furthermore, the problem of a cylindrical hole in plane strain under uniaxial remote tension has been investigated. The same material parameters used for the example discussed above were taken and the results for  $\sigma_{\varphi\varphi}^{\max+}/\sigma_0$  are shown in Fig. 4.

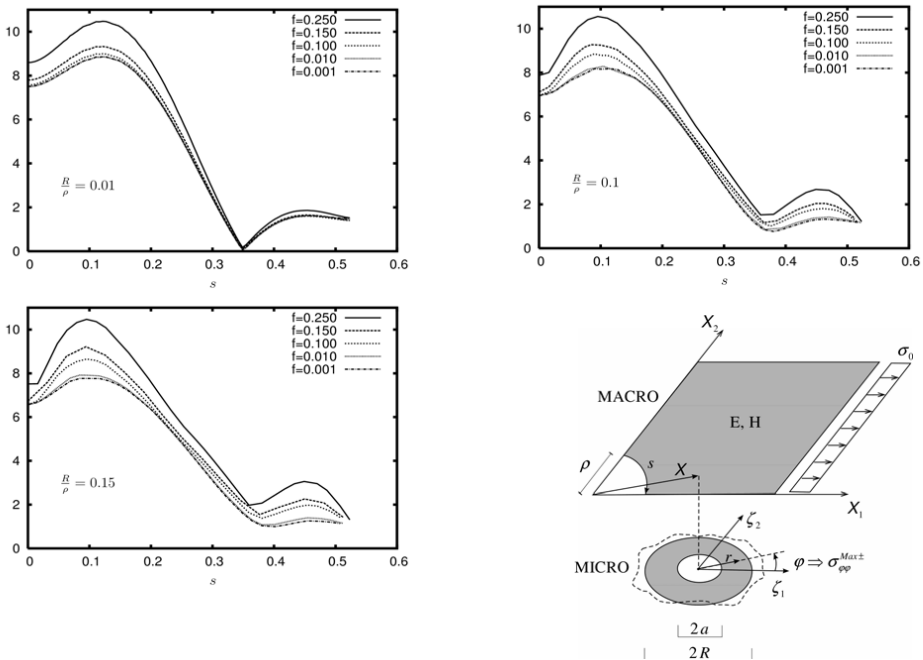


Figure 4:  $\sigma_{\varphi\varphi}^{\max+}/\sigma_0$  for uniaxial tension as function of the arc length  $s$ , varying  $f$  and  $R/\rho$

Again, it turns out that for a given void volume fraction a coarse micro structure is more strength than a dense micro structure. The maximum values for  $\sigma_{\varphi\varphi}^{\max+}/\sigma_0$  and  $|\sigma_{\varphi\varphi}^{\max-}|/\sigma_0$  are shown for all performed simulations in Fig. 5, where the results for biaxial and uniaxial remote tension are found on the left hand and on the right hand side, respectively..

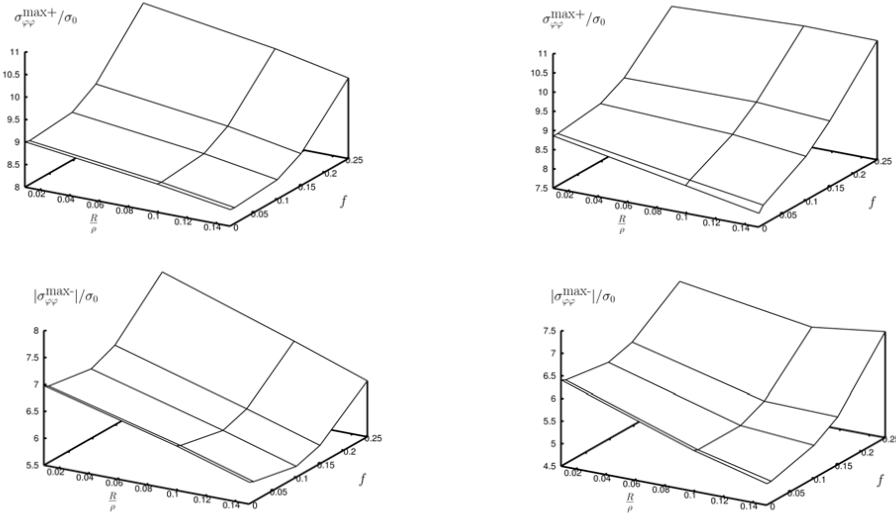


Figure 5: Maximum values for  $\sigma_{\varphi\varphi}^{\max+}/\sigma_0$  and  $|\sigma_{\varphi\varphi}^{\max-}|/\sigma_0$  for biaxial and uniaxial remote tension

As a third example, a compression test performed with a long cylindrical bar is considered. The experimental setup is shown together with the finite element mesh used for all calculations in Fig. 6. Plane strain conditions were assumed and the simulations were performed using contact in conjunction with friction and small sliding. The same values as used before were taken for E and  $\nu$ . The void volume fractions  $f$  were taken from the set (0.001, 0.01, 0.1). Here,  $\rho$  is the radius of the cylindrical bar as depicted in Fig. 6 and for the ratios between the half spacing of the micro-voids and  $\rho$  the values 0.001, 0.1 and 0.1 were chosen. These values correspond to micro structures with approximately 500, 250 and 50 micro-voids, respectively, along the radius of the cylinder.

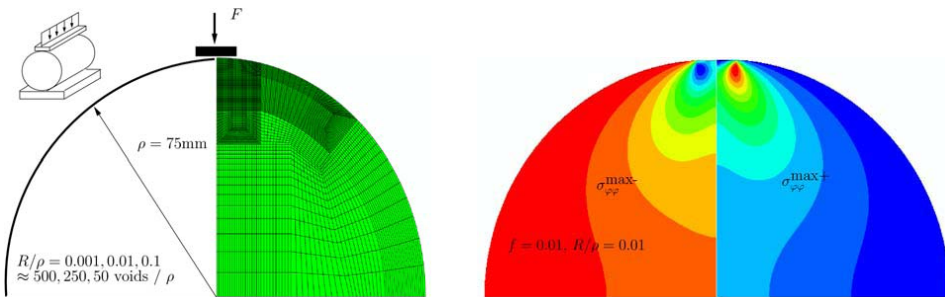


Figure 6: Compression test: experimental setup, finite element discretization and distributions of  $\sigma_{\varphi\varphi}^{\max+}$  and  $\sigma_{\varphi\varphi}^{\max-}$  for  $f=0.01$  and  $R/\rho=0.01$

The failure criteria have been evaluated and the results for  $\sigma_{\varphi\varphi}^{\max+}/F$  and  $\sigma_{\varphi\varphi}^{\max-}/F$  are shown for all performed simulations in Fig. 7, where  $F$  is the applied load as shown in Fig. 6. Surprisingly, the failure criteria predict that the lower the values for  $R/\rho$  the more strength the considered structure has, which is contrary to the results obtained for the plate with hole under remote tension.

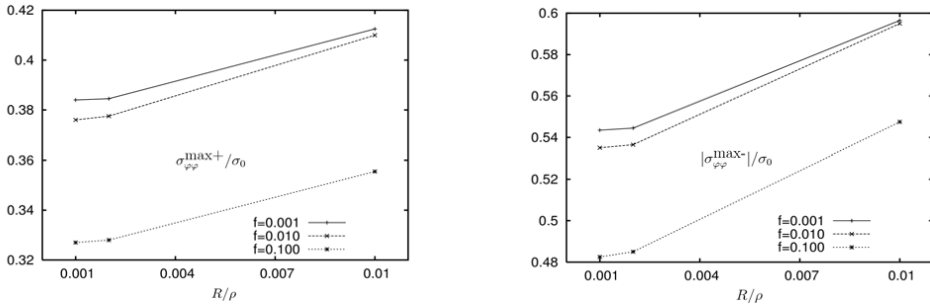


Figure 7: Maximum values for  $\sigma_{\varphi\varphi}^{\max+}/\sigma_0$  and  $|\sigma_{\varphi\varphi}^{\max-}|/\sigma_0$  obtained for the compression test

### Summary and Outlook

Strain gradient theory has been applied in order to simulate size effects in the failure of structures consisting of porous elastic materials. The results obtained for the considered examples indicate that size effects in failure depend not only on the micro structural properties but also on the macroscopic geometry and loading conditions. The failure criteria used here were chosen without experimental background and therefore more or less arbitrarily based on the maximum hoop stress at the micro-voids. It was shown that size effects can be reflected in principle. However, other criteria based on maximum shear stress inside the RVE or energetic criteria may be formulated as easily and further investigations in conjunction with corresponding experiments are necessary in order to validate the approach.

Furthermore, testing of porous elastic materials like e.g. aircrete is performed mostly by means of compression tests with cubes. However, without variations of the microstructural properties throughout the considered specimen, size effects could not be predicted by the approach presented here because of the absence of gradients in the macroscopic fields. Therefore, the strain gradient model has to be combined with a statistical approach, accounting this way for variations of the microstructure in the specimens.

### References

- [1] Th. Schneider: Modellierung der Festigkeit poröser Keramiken, PhD thesis (2001), Universität Erlangen-Nürnberg
- [2] E.K. Kunhanandan Nambiar, K. Ramamurthy: Cement and Concrete Research Vol. 37 (2007), p. 221
- [3] R.S. Lakes: Int. J. Solids Struct. Vol. 22 (1) (1986), p.55
- [4] R.D. Mindlin: Arch. Rat. Mech. Anal. Vol. 16, (1964), p. 51
- [5] R.D. Mindlin, N.N. Eshel: Int. J. Solids Struct. Vol. 4 (1) (1968), p. 109
- [6] R.A. Toupin: Arch. Rational Mech. Anal. Vol 11 (1962), p. 385

- [7] L. Zybell, U. Mühlich and M. Kuna: Arch. Appl. Mech. (2008) DOI 10.1007/s00419-008-0238-1
- [8] M. Gologanu, J. Leblond, G. Perrin and J. Devaux, in: CISM-Courses and Lectures: International Centre For Mechanical Science Series, p. 61 (1997)
- [9] S. Forest in: Geometry, Continua and Microstructure, Herrmann, Paris (1999), p. 35-48
- [10] Abaqus Version 6.6 Documentation, Hibbit, Karlsson and Soerensen (2005)
- [11] J.Y. Shu, W.E. King and N.A. Fleck: Int. J. Numer. Meth. Eng. Vol. 44 (1999) , p. 373
- [12] L. Zybell: Implementation of a user-element considering strain gradient effects into the FE-program Abaqus, Master's thesis, TU-Bergakademie Freiberg (2007),